Low Frequency Sound Field Reconstruction in Non-rectangular Room: A Numerical Validation

Thach Pham Vu
Signal processing laboratory LTS2, EPFL, Lausanne, Switzerland

Etienne Rivet
Signal processing laboratory LTS2, EPFL, Lausanne, Switzerland

Herve Lissek
Signal processing laboratory LTS2, EPFL, Lausanne, Switzerland

Summary
Characterization of sound fields in rooms has always been a challenging task. A faithful reconstruction of sound fields in rooms generally would require an impractically high number of microphones. At low frequencies, where sound field can be modeled as a finite superposition of modes, a combination of Matching Pursuit (MP) and Least-squares optimization can help interpolate the Room Impulse Responses using a relatively small number of measurements. Our research focuses on using this paradigm to obtain the low-frequency information of a room in a broader sense, where the spatial distribution of sound pressure in a non-rectangular reverberating room can be reconstructed and visually analyzed. Several evaluations are performed along the progression of the framework to confirm its validity. The modal parameters estimated by MP are also compared with those obtained by the Rational Fraction Polynomial method (global curve fitting). Finally, the reconstruction of sound field, which leads to the visualization of the spatial distribution of sound pressure at any chosen frequency in the range of study, is validated visually and numerically using a finite element method software for a non-rectangular room model. This demonstration provides an extensive look at the high robustness and reliability of the framework as a whole, which is crucial in terms of its practical implementations for room acoustics practitioners.

PACS no. 43.50.+y, 43.58.+z, 43.60.+d

1. Introduction

Room Frequency Response (RFR) and its time domain equivalent, Room Impulse Response (RIR) express the acoustic transmission characteristics between a source and a receiver in a room. Characterization of sound fields in a room, depending on different purposes, requires a thorough knowledge of either the RIRs or RFRs of the room with varying receivers' and/or speakers' position. Sound field reconstruction of a room is a process that gathers a limited number of measurements in the room and through different methods, reconstructs the entire enclosed sound field. The challenge here is to achieve accurate sound field reconstruction with the least possible measurements.

A precise reconstruction of sound fields in rooms using a regular space and time sampling would typically result in a dense microphones placement. With this knowledge in mind, the research in [1] has been able to reduce the number of measurement points by looking into the sparse spectrum of the Plenacoustic Function, which for a 3D spatial problem, is enclosed inside a 4D hypercone. More recently, it has been shown in [2] that the RIRs can be interpolated using a reduced number of measurement points through Compressive Sensing (CS) by considering certain sparsities that exist in room acoustics at low frequency. Several experiments and simulations have been performed to analyze the accuracy and efficiency of the compressive sensing framework in interpolating the RIRs [2],[3]. Many of these tests are with regards to the interpolation RIRs close to the center of the arrays.

In this paper, we focus on using this suggested CS paradigm to obtain the low frequencies information of a room under an extensive point of view, where the spatialization of sound pressure in a general non-rectangular room can be reconstructed and visually analyzed using numerical simulation. Along the progression of the algorithm, the estimated modal parameters are also compared with the reference. Through

these analysis, the performance of the CS framework can be assessed to verify its validity and robustness under different circumstances.

The outline of the paper is as follows. First, we briefly tackle the sparse properties that are present in room acoustics at low frequencies in Section 2. The CS reconstruction framework composed of the Simultaneous Orthogonal Matching Pursuit (SOMP) and Least-square estimation method can then be explained in Section 3. Section 4 is dedicated towards the validation of the framework in reconstructing the sound field in the room. In particular, the first part of the analysis compares the modal parameters estimation used in the CS framework with the numerical results from Finite Element Method (FEM) simulations. The estimations are then further compared with the results produced by another modal estimation method which makes use of the Rational Fraction Polynomial (RFP) in global curve-fitting. The second part focuses on the reconstruction of the sound field of the room using the responses interpolated by the CS framework. This can be done by assessing the RFR, which is the frequency domain counterpart of the RIR. With the RFRs, it is possible to reconstruct the sound pressure distribution in the room at any particular frequency of interest. A comparison between the reconstructed sound fields and the numerical results are then performed to confirm the validity and robustness of the framework. Finally, some concluding remarks are presented in Section 5.

2. Sparsities in room acoustics

A. Modal decomposition

In low frequencies, the acoustic wave equation can be decomposed as a discrete sum of damped harmonic eigenmodes:

$$p(t,\vec{X}) = \sum_{n\in\mathbb{Z}^*} A_n \Phi_n(\vec{X}) g_n(t) \tag{1}$$

where Φ_n is the mode shape (or eigenfunction), $g_n(t)$ is the time dependent harmonic decaying function and A_n is the corresponding complex expansion coefficient of mode n. Each eigenmode is uniquely represented by a complex wavenumber $k_n = (\omega_n + j\delta_n)/c_0$ where ω_n is the angular frequency and $\delta_n > 0$ is the damping coefficient of the mode. The harmonic decaying function $g_n(t)$ can then be expressed as:

$$g_n(t) = e^{jk_n c_0 t} = e^{j(\omega_n + j\delta_n)t} = e^{j\omega_n t} e^{-\delta_n t} \tag{2}$$

Note that while we do observe the existence of $\vec{X}$ in (1) which is the position of the receiver, we have not seen the presence of the source and its properties. This information is in fact included in the complex coefficients A_n's and will remain so for the rest of our derivation. In here, we only consider the set-up with one fixed source in the room and the objective is to reconstruct the whole sound pressure field in this limiting case.

The mode shape function, on the other hand, is a space dependent function. In the case of ideally rigid walls, each mode shape function Φ_n is the exact solution of the Helmholtz equation [4]:

$$\Delta\Phi_n + k_n^2 \Phi_n = 0 \tag{3}$$

In the case of non-rigid walls, it can be assumed that the above equation holds for positions not too close to the wall and in the case of rooms with low wall damping. The expansion of the mode shape functions will be performed in the next section.

B. Mode shape approximation

The derivation in the previous section poses a form of structured sparsity which is based on the discrete modal decomposition of the sound pressure in low frequencies. It can be seen that the mode shape functions Φ_n's need to be linked directly to the position of the receiver ($\vec{X}$). In [5] it has been shown that the mode shape functions can be approximated based on the premise of spherical harmonics and spherical Bessel functions. According to this, the mode shape function can be approximated by a finite sum of plane waves sharing the same wavenumber pointing in various directions. The individual mode shape, hence, can be formulated using the R-th order approximation:

$$\Phi_n(\vec{X}) \approx \sum_{r=1}^{R} B_{n,r} e^{j\vec{k}_{n,r}\cdot\vec{X}} \tag{4}$$

where $\vec{k}_{n,r}$'s are the 3D wavevectors sharing the same wavenumber $||\vec{k}_{n,r}||_2 = |k_n|$. Note that this, in contrast of the exact sparsity in the previous section, is an approximated sparsity. This plane waves summation not only gives a good approximation of the mode shape, but more importantly, makes it possible to have a closed-form interpretation of the mode shape function regardless of the type of the modes in the room. Assuming now that for a chosen frequency limit, a value of R number of wavevectors would be enough to closely approximate every mode shape function within this limit, using (2) and (4), the equation in (1) could be expanded as:

$$p(t,\vec{X}) = \sum_{n,r} C_{n,r} e^{j\omega_n t} e^{-\delta_n t} e^{j\vec{k}_{n,r}\cdot\vec{X}} \tag{5}$$

where $C_{n,r} = A_n B_{n,r}$. As can be seen, through a series of derivations, the space time equation in (1) can now be interpreted as the sum of space-time damped harmonics with the expansion coefficients $C_{n,r}$'s. This expansion form of the equation could be in fact interpreted in multiple ways under the matrix form, which is ideal for the CS framework in the next section.

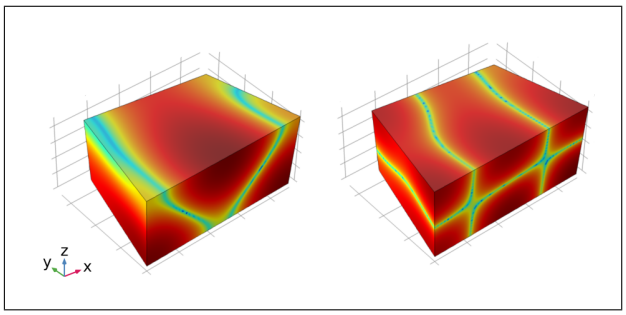

Figure 1. Typical room modes for a non-rectangular room

3. Compressive sensing framework

3.1. The inputs

The algorithm in this research directs towards a general case, where the room though still has 6 walls (including ceiling and floor), is however non-rectangular and hence the modal behavior of the room would be more difficult to predict (Fig. 1). Inside this room, a number of M microphones will be randomly placed in different positions in order to acquire the RIR measurements. These unprocessed RIRs can then go through a low pass filter and be down-sampled based on the frequency range of interest in order to reduce the computational cost later on in the algorithm. Calling N_t the length of the time vector for these processed RIRs, we will end up with an $(N_t \times M)$ matrix $\mathbf{S}$ of signals which will be taken as the input of our algorithm.

3.2. The outputs

In short, the output of the algorithm should be all the unknowns in (5) except pre-chosen parameters such as the number of modes N and the wavevectors $\vec{k}_{n,r}$ for each mode shape approximation (as can be seen later, is the result of uniform sampling a sphere without prioritizing any direction). Therefore, the outputs include the angular eigenfrequency ω_n and damping δ_n of each mode as well as the $N \times R$ expansion coefficients $C_{n,r}$. With all these values found, we can interpolate the RIRs at any position $\vec{X}_{int}$ by simply plugging it into equation (5).

3.3. Algorithm

The algorithm can be divided into two main parts. The first part is making use of the Matching Pursuit regimes to find the wavenumbers k_n's for the N room modes. With these results, the second part focuses on using the least-squares method to approximate the expansion coefficients $C_{n,r}$ for a set of predefined wavevectors $\vec{k}_{n,r}$.

A. Wavenumber identification

This initial step is largely based on the Simultaneous Orthogonal Matching Pursuit method [6] (SOMP) for damped sinusoids [7]. This particular method can estimate damped sinusoidal components that are highly matched with the input signals from a redundant set of sinusoids. At the beginning, two sets of $\omega_{min} < \omega < \omega_{max}$ and $\delta_{min} < \delta < \delta_{max}$ can be formed. The range of these sets are based on pre-acquired knowledge of the room such as its reverberation time and the geometrical properties. The limit values at two ends of each set do not have to be precise but should rather be an estimation. Forming all possible combination between the entries from these two sets will now produce an overly redundant set of complex components $(j\omega_q - \delta_q)$ in which $q \in [1, Q]$ with Q as the total number of possible combinations between ω and δ. Here, the word 'overly redundant' is to suggest that only a small number of entries from this set are the correct eigenfrequency and damping of the modes in the room. Each entry of this set can then be used to form a time vector of length N_t of damped sinusoid $\underline{\theta_q} = e^{j\omega_q t}e^{-\delta_q t}$. Now, using the normalized vectors $\overline{\theta_q} = \underline{\theta_q}/||\underline{\theta_q}||_2$ as columns, we have an $(N_t \times Q)$ matrix $\overline{\Theta}$.

The algorithm, in short, will repetitively perform a pole searching procedure in loops. Each loop begins with an $(N_t \times M)$ residue matrix $\mathbf{R}_i$. At the first loop, $\mathbf{R}_1$ is set to be equal to the predefined signal matrix $\mathbf{S}$. Through the pole searching procedure, a damped sinusoid with the highest correlation to the residue matrix (represents a pair of ω_n and δ_n) is chosen. The residue matrix $\mathbf{R}_{i+1}$ of the next loop can then be formed by extracting the contribution of this chosen sinusoid from $\mathbf{R}_i$. The stages of a loop can be seen below:

- Define a $(Q \times M)$ correlation matrix $\Xi_i = |\overline{\Theta}^H \mathbf{R}_i|$. Each row indexed q of Ξ_i represents a set of M correlation values between the q^{th} normalized damped sinusoid with each of the M measurements. Adding up the energy of this set of values gives us a representative correlation value σ_q between the q^{th} damped sinusoid with the entire set of RIR measurements: $\sigma_q = \sum_{m=1}^{M}(\Xi_{i[q,m]})^2$. Out of the Q values of σ_q, we choose the maximum one, which corresponds to the pole with the highest correlation to our measurements. Consequently, its index (namely, q_i) points to the resulting chosen modal wavenumber of this loop which is $k_i = (\omega_{q_i} + j\delta_{q_i})/c_0$.
- After finding a pole, following the orthogonalization and projection of SOMP in [6], the residue matrix for the next loop can be interpreted as $\mathbf{R}_{i+1} = \mathbf{R}_i - \mathcal{P}_i\mathbf{R}_i$ in which $\mathcal{P}_i$ is the projection matrix onto the chosen damped sinusoidal from the previous step.
- Repeat with $i = i + 1$ until $i = N$

At the end of the process, we have a group of complex wavenumbers that corresponds to the eigenmodes of the room.

Besides SOMP, there are other methods that can be used to acquire the modal parameters of a room. One particular example is the global curve-fitting method in the frequency domain using the Rational fraction polynomial (RFP) form. This has been used in [8] to estimates the modal parameters by curve fitting the RFR measurements. Regular curve fitting methods are usually done locally, meaning to perform on a single function at a time. The RFP method in [9], on the other hand, performs curve-fitting procedures on multiple-point frequency response functions at the same time to estimate the model of the system. It assumes that the frequency response functions are linear and can be modeled as a ratio of two polynomials, where the denominator is the same for all the frequency responses. The poles in the denominators (which contain information on the eigenfrequencies and modal damping) are then found by curve-fitting simultaneously the given frequency response functions. Finally, through local curve-fitting of the numerator with the individual responses and using the numerical fraction expansion, the residue (mode shape component) for each mode of each frequency response can be estimated.

B. Projection onto wavevectors

After the previous framework, we have been able to find the ω_n's and δ_n's given in equation (5). The remaining parameters to be found are the expansion coefficients $C_{n,r}$'s.

- The first stage is the separation of the current known and unknown parameters in terms of matrices. The temporal terms in (1) are now known and can be separated. Writing in matrix form with regards to the measurement matrix $\mathbf{S}$, we have: $\mathbf{S}^{\mathrm{T}} = \Psi G$ with G is the $(N \times N_t)$ matrix with each of its row a modal damped sinusoidal $g_n(t) = e^{j\omega_n t}e^{-\delta_n t} = e^{jk_n t}$ and Ψ is the $(M \times N)$ space-dependent matrix of modes with the inclusion of the expansion coefficients A_n's that appear in (1):
$$\Psi_{[m,n]} = A_n \Phi_n(\vec{X}_m) \tag{6}$$
with $\vec{X}_m$'s the M position vectors for the input measurements of $\mathbf{S}$. One way of looking at (6) is that if $N_t > N$ (which usually is the case), it poses an overdetermined matrix problem with $(M \times N)$ unknown and $(M \times N_t)$ equations. Hence, we can estimate the $(M \times N)$ matrix of Ψ by computing the least-squares estimation:
$$\Psi \approx \mathbf{S}^{\mathrm{T}} G^H (GG^H)^{-1} \tag{7}$$
- Next, based on the derivation in (5) we can expand Ψ further in terms of plane waves expansion:
  - First, we have to specify the component wavevectors. For each wavenumber, we create a set of R wavevectors $\vec{k}_{n,r}$ whose lengths and directions correspond to a uniform sampling of a sphere with radius $|\omega_n/c_0|$ (according to [2],[10], a value of $R \approx 3M/4$ is sufficient to avoid both over and under-fitting of the data).

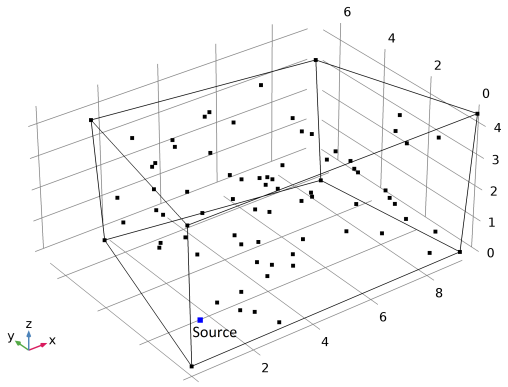

Figure 2. Geometry of the FEM model. The black dots represent the measurement points.

  - Each column ψ_n of the matrix Ψ can now be analyzed individually as they belong to different modes. If ρ_n is specified as the $(M \times R)$ matrix of the plane wave harmonics for mode n in which $\rho_{n[m,r]} = e^{j\vec{k}_{n,r}\cdot\vec{X_m}}$, then we can express individually each column vector ψ_n as:
$$\psi_n = \rho_n \mathbf{C}_n \tag{8}$$
where $\mathbf{C}_n$ is the $(R \times 1)$ vector containing all the R expansion coefficients $C_{n,r}$ of mode n. With $M > R$ as previously chosen, taking ρ_n as the basis, we can perform a least-squares projection of ψ_n onto this basis to find the coefficient vector $\mathbf{C}_n$:
$$\mathbf{C}_n \approx (\rho_n^H \rho_n)^{-1} \rho_n^H \psi_n \tag{9}$$
Repeating this procedure across every existing mode $n \leq N$ will return all the expansion coefficients needed for reconstruction.

4. Numerical Validation

In this section, an FEM model of a non-rectangular room is first introduced for numerical analysis. The simulation results are then used as the inputs for the reconstruction framework suggested in the previous section. At the same time, they can also be used as a reference to validate the reconstruction result. The validation of the framework starts by evaluating the modal parameters estimation by SOMP. The resulting eigenmodes are compared to both the reference as well as the estimation results using the aforementioned RFP method. The entire framework is then validated through the comparison of RIR/RFR and most importantly, the comparison of the sound field reconstruction where the spatial distribution of sound pressure can be assessed.

4.1. Numerical simulation

The numerical simulation is performed using a Finite Element Method (FEM) analysis. The model is a non-rectangular room with maximum height of 4.5m, maximum width of 9.6m and maximum length of 6.8m

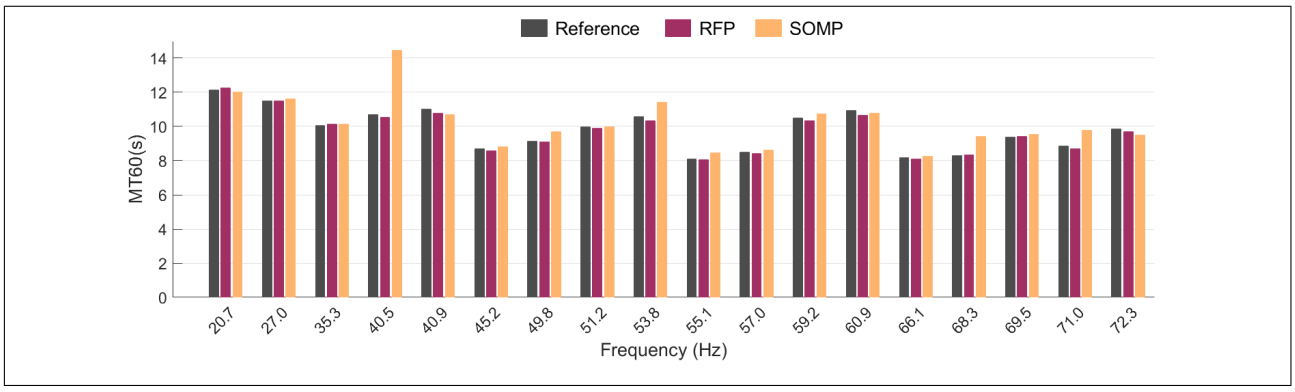

Figure 3. Modal decay times of the non-rectangular reverberant room estimated from the SOMP and RFP methods in comparison with FEM analysis.

which replicates the actual reverberation chamber of our laboratory. The damping of the walls are kept to be low, approaching that of a reverberation chamber. The source is chosen to be a monopole point source and is put in proximity to one corner of the room. The 70 measurement points are spread randomly around the room (refer to Fig. 2). As the test of validity of the algorithm is of importance in this research, the number of microphones is chosen to be moderately high to acquire fairly accurate results without hindering the computation in terms of processing time and memory.

In our numerical analysis, the frequency range is chosen to be below 100 Hz where around 40 eigenmodes exist within this range. The processed RIRs will go through the series of algorithm detailed in the compressive sensing framework and will return 45 complex wavenumbers along with the gains for the 53 ($\approx 3M/4$) wavevectors for each of these wavenumbers. The reason we use 45 as the number of mode is to be consistent with the practical case where an exact number of modes under a chosen frequency limit could not usually be precisely predicted, especially in case of a non-rectangular room.

4.2. Modal parameters estimation

In this section, we evaluate the first half of the reconstruction framework regarding modal parameters estimation. The comparison is performed regarding the two properties commonly used in modal analysis: eigenfrequency (f_n) and the modal decay time (MT_{60n}) which is defined as:

$$\mathrm{MT}_{60n} = \frac{3\ln(10)}{\delta_n} \tag{10}$$

The modal decay times estimated from SOMP and RFP methods for the first 18 modes of the room are compared with those computed from the FEM analysis (see Fig. 3). Because of the minimal difference between the three results in terms of modal frequency values, we focus on comparing the modal decay time which is directly related to the damping of each mode. As can be seen from the figure, both the RFP and SOMP method perform well in terms of eigenmodes identification except the fact that SOMP underestimates the damping at 40.5 Hz which will be discussed later.

Generally, we can observe that the RFP method performs mildly better than SOMP. However, it is worth mentioning that for RFP method, if the number of modes within a frequency range is not absolutely precise, it takes a lot of trial and error in order to come up with a coherent curve-fitting results in the end. Although, both RFP and SOMP require the users' input on how many modes they want to find, this vulnerability does not occur to SOMP. This is due to the fact that the room modes are found in RFP simultaneously whereas in SOMP they are found in series: the room modes that have the highest contributions to the signals will be found first and then come the ones with less. This gives SOMP an advantage in terms of robustness as the results do not deviate much from reality even if the users underestimate or overestimate the number of modes within the frequency range of interest. The number the users enter can only change how many loops the algorithm repeats itself but does not change the result of each individual loop.

The underestimated damping at 40.5 Hz from SOMP also comes from the fact that our algorithm runs in loops. As after every loop, the energy of the residue will be reduced more and more, the modes that are found at the far end of the algorithm are prone to higher errors than the ones found around the very first loops. In our algorithm, the mode at 40.5 Hz is found at the 37^{th} loop and hence could be less accurate than some others that are found earlier. The same situation also occurs when users overestimate the number of modes. Then, around the final loops, the algorithm will certainly find some frequencies that do not correspond to any mode. However, as the algorithm proceeds in a residual manner, this, same as the 40.5 Hz error, has minimal effects to the reconstruction happening in the next stage because the contributions of the few mismatched modes are

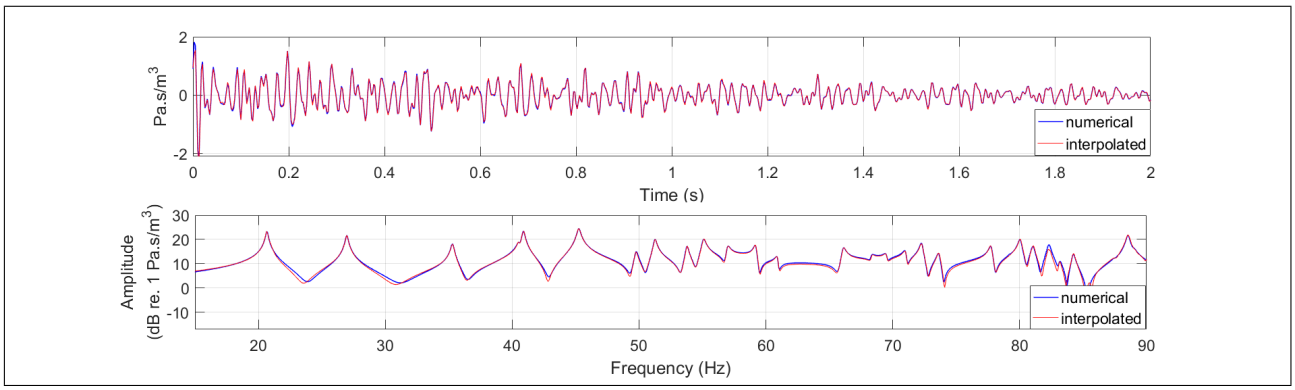

Figure 4. Interpolation of the RIR and RFR for a point inside the room.

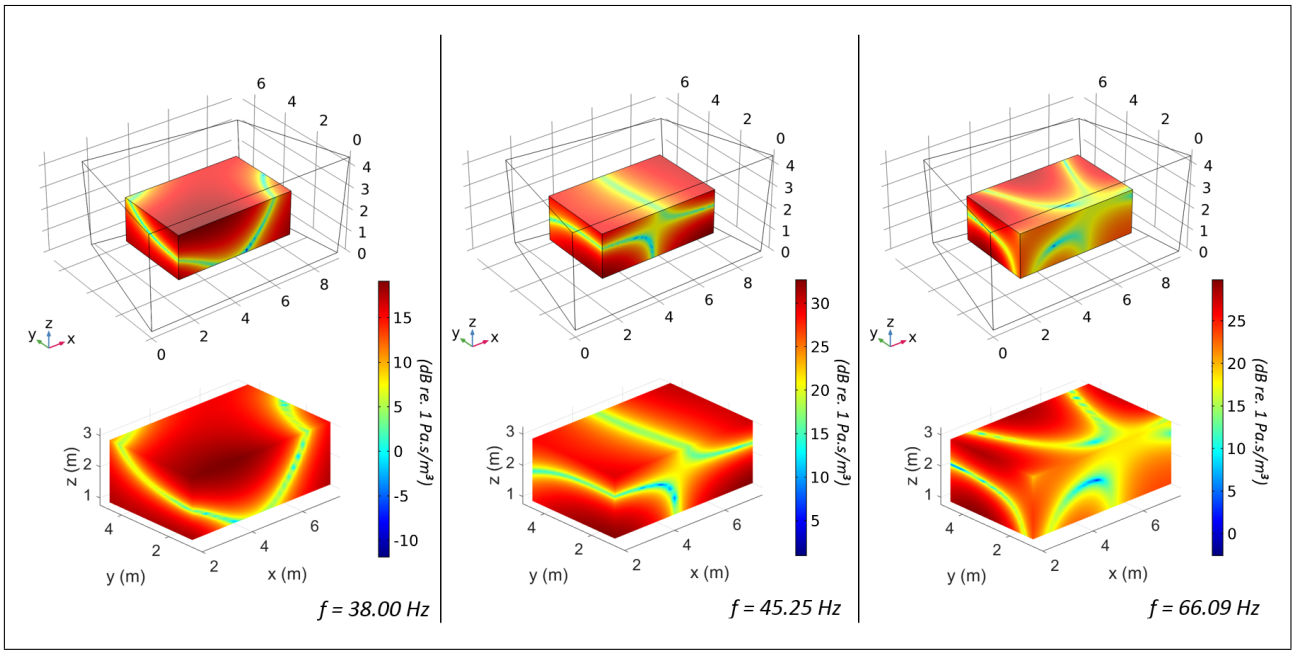

Figure 5. Sound field reconstruction (bottom) at different frequencies for a rectangular area inside the room in comparison with the referencing sound fields from numerical simulation (top).

usually small comparing to the correct ones. This can further be seen later on in the reconstruction results.

4.3. Sound field reconstruction

A. Local interpolation

Using the outcomes of the algorithm, it is now possible to interpolate the RIR at any point inside the geometry. The RIRs in our case indicate the transmission between the source volume flow rate (in m^3/s) and the sound pressure (in Pa) acquired at the measurement points. An example can be seen in Fig. 4 for a point far from the walls but also not too close to the center of the room. It can be observed that for 70 measurement points, the reconstruction is highly accurate for both the RIR and RFR in this example. It should be noted, however, that this high accuracy is not guaranteed for every interpolated point in the room and the error could be higher depending on the position of the point and in relation with the precision of the eigenmodes searching results. This, once again, highlights the need for a spatial representation of the sound field to confirm the validity of the framework in general.

B. Spatial sound pressure distribution

The interpolation process can now be done for multiple points to acquire a series of RIRs for the room. The RFRs of the room can then be produced through the Fourier transform of these RIRs. These resulting RFRs will allow us to observe the spatial response of the room at any single frequency of interest.

It has been studied in [4] that for a room with non-rigid walls, the Helmholtz equation for eigenmode is less valid for positions close to the walls. Hence, our first visualization is for a rectangular volume inside the room but away from its walls. This reconstruction can be compared with a frequency domain study

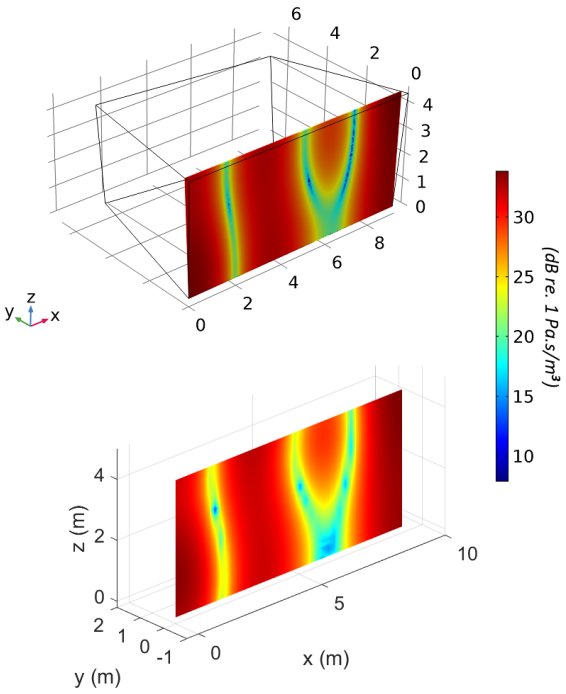

Figure 6. Comparison of the reconstruction framework on a surface close to the wall at an eigenfrequency $f = 59.18$ Hz (bottom) with the numerical simulation result (top).

using the same settings in FEM analysis (refer to Fig. 5). It can be observed that the reconstruction of the sound field using CS yields highly accurate results. Through this visualization of sound pressure, we can confirm that the algorithm not only performs well on a few interpolated positions but it is also capable of reconstructing the sound field accurately over wide areas. The presence of the mode shapes can also be clearly observed in all three examples. Furthermore, the high level of accuracy is maintained in every direction of the 3D depiction since the input measurement points are spread randomly in the room. A few initial tryouts with a regular grid of microphones have not achieved such global precision in the reconstruction. This, once again emphasizes the advantage of the much-recommended randomness in common CS frameworks. From Fig. 5, it should also be noticed that although there might be small differences when comparing point by point, the general shapes as well as the separation between high and low sound pressure areas are nevertheless precisely depicted. It could also be observed in the comparison that the depiction of sound pressure field is accurate not just for the eigenfrequencies (at 45.25 Hz and 66.09 Hz) but also for frequencies in between two consecutive modes (38 Hz is an example).

Next, we reconstruct the spatial pressure distribution on a surface close to one of the walls to analyze the near-wall performance. We can confirm that the reconstructed sound field, in general, maintains the same level of accuracy for a wide range of frequencies. There are a few cases, like the one in Fig. 6 where the reconstruction tends to have slightly higher errors but the general patterns of the sound pressure distribution are nevertheless identical with the reference. This shows that for lightly damped room, the near-wall performance of the reconstruction can yet still be valid but is slightly less accurate comparing to regions further away from the walls. Future studies will focus on cases with highly damped walls to test the limit of the reconstruction.

5. Conclusion

In this paper, we have been able to show the validity of the compressive sensing approach in reconstructing sound fields of a non-rectangular room. The framework has been able to reconstruct the spatial sound pressure field inside the room at certain frequencies and analyze its precision in comparison to that from numerical simulations. The comparisons show promising results both for the areas away from and close to the walls. This could prove to be useful for further application of the algorithm by a wider audience of users. One of many potential applications is to use this method to evaluate the change in the sound fields due to different room mode treatment methods. Future studies will focus on this particular application as well as study further on other robust aspects of the algorithm such as its accuracy in highly damped rooms and how to compensate for it. Along the progression of the framework, with regards to room modes identification, the research has also compared two pole-searching-based methods of RFP and SOMP in terms of accuracy and robustness. One advantage of the RFP method is its fast computation time but it is with the cost of low robustness and the liable low accuracy caused by wrong estimation of number of modes. The possibility of combining these two methods to take advantage of their strengths and to compensate for the existing weaknesses can also be an interesting subject for future research.

References

[1] T. Ajdler, L. Sbaiz and M. Vetterli, "The Plenacoustic Function and Its Sampling," in IEEE Transactions on Signal Processing, vol. 54, no. 10, pp. 3790-3804, Oct. 2006.

[2] R. Mignot, G. Chardon and L. Daudet, "Low Frequency Interpolation of Room Impulse Responses Using Compressed Sensing", in IEEE/ACM Transactions on Audio, Speech, and Language Processing, vol. 22, no. 1, pp. 205-216, Jan. 2014.

[3] H. Peic Tukuljac, T. Pham Vu, H. Lissek, and P. Vandergheynst (in press), "Joint estimation of room geometry and modes with compressed sensing", in IEEE International Conference on Acoustics, Speech and Signal Processing (ICASSP), 2018.

[4] H. Kuttruff, 2000. Room acoustics Fourth. Spon Press.

[5] A. Moiola, R. Hiptmair, and I. Perugia, "Plane wave approximation of homogeneous Helmholtz solutions", Zeitschrift fur Angewandte Mathematik und Physik (ZAMP), vol. 62, pp. 809-837, 2011.

[6] Joel A. Tropp, Anna C. Gilbert, Martin J. Strauss, "Algorithms for simultaneous sparse approximation. Part I: Greedy pursuit, Signal Processing", Volume 86, Issue 3, 2006, Pages 572-588, ISSN 0165-1684, https://doi.org/10.1016/j.sigpro.2005.05.030.

[7] G. Chardon and L. Daudet, Optimal subsampling of multichannel damped sinusoids, in Proc. 6th IEEE Sensor Array and Multichannel Signal Process. Workshop (SAM'10), pp. 25-28, 2010.

[8] E. Rivet, S. Karkar, H. Lissek, T. N. Thorsen, & V. Adam, (2016, May)."Experimental assessment of low-frequency electroacoustic absorbers for modal equalization in actual listening rooms." Audio Engineering Society Convention 140. Audio Engineering Society, 2016.

[9] Richardson M. H., Formenti D. L., "Global Curve Fitting of Frequency Response Measurements using the Rational Fraction Polynomial Method", 3RD IMAC Conference, Orlando, FL, January 1985

[10] R. Roy and T. Kailath, "Estimation of signal parameters via rotational invariance techniques," IEEE Trans. Acoust., Speech, Signal Process., vol. 37, no. 7, pp. 984-995, 1989.